Daily Satellite Observations of Nitrogen Dioxide Air Pollution Inequality in New York City, New York and Newark, New Jersey: Evaluation and Application

AUTHOR NAMES: Isabella M. Dressel[1], Mary Angelique G. Demetillo[1], Laura M. Judd[2], Scott J. Janz[3], Kimberly P. Fields[4], Kang Sun[5,6], Arlene M. Fiore[7], Brian C. McDonald[8], and Sally E. Pusede[1]*

AUTHOR ADDRESSES:

[1]Department of Environmental Sciences, University of Virginia, Charlottesville, VA 22904, USA

[2]NASA Langley Research Center, Hampton, VA 23681, USA

[3]NASA Goddard Space Flight Center, Greenbelt, MD 20771, USA

[4]Carter G. Woodson Institute for African American and African Studies, University of Virginia, Charlottesville, VA 22904, USA

[5]Department of Civil, Structural and Environmental Engineering, University at Buffalo, Buffalo, NY 14260, USA

[6]Research and Education in eNergy, Environment and Water (RENEW) Institute, University at Buffalo, Buffalo, NY 14260, USA

[7]Department of Earth, Atmospheric and Planetary Sciences, Massachusetts Institute of Technology, Cambridge, MA 02139, USA

[8]Chemical Sciences Laboratory, NOAA Earth System Research Laboratories, Boulder, CO 80305, USA

*Corresponding author: sepusede@virginia.edu

Abstract. Urban air pollution disproportionately harms communities of color and low-income communities in the U.S. Intraurban nitrogen dioxide (NO_2) inequalities can be observed from space using the TROPOspheric Monitoring Instrument (TROPOMI). Past research has relied on time averaged measurements, limiting our understanding of how neighborhood-level NO_2 inequalities co-vary with urban air quality and climate. Here, we use fine scale (250 m x 250 m) airborne NO_2 remote sensing to demonstrate daily TROPOMI observations resolve a major portion of census tract-scale NO_2 inequalities in the New York City–Newark urbanized area. Spatiotemporally coincident TROPOMI and airborne inequalities are well correlated (r = 0.82–0.97), with slopes of 0.82–1.05 for relative and 0.76–0.96 for absolute inequalities for different groups. We calculate daily TROPOMI NO_2 inequalities over May 2018–September 2021, reporting disparities of 25–38% with race, ethnicity, and/or household income. Mean daily inequalities agree with results based on TROPOMI measurements oversampled to 0.01^{o} x 0.01^{o} to within associated uncertainties. Individual and mean daily TROPOMI NO_2 inequalities are largely insensitive to pixel size, at least when pixels are smaller than ~60 km^2, but are sensitive to low observational coverage. We statistically analyze daily NO_2 inequalities, presenting empirical evidence of the systematic overburdening of communities of color and low-income neighborhoods

with polluting sources, regulatory ozone co-benefits, and worsened NO_2 inequalities and cumulative NO_2 and urban heat burdens with climate change.

Synopsis. Daily TROPOMI satellite observations resolve a majority of intraurban NO_2 inequalities in New York City and New Jersey; NO_2 inequalities covary with air quality and climate variables

Keywords. Urban air pollution, environmental justice, nitrogen dioxide, satellite measurements, TROPOMI

1 INTRODUCTION

New York City, New York and Newark, New Jersey are populous U.S. cities with poor air quality, where there are documented inequalities in air pollution concentrations and health impacts affecting communities of color and low-income residents.[1-7] There have been decades of community organizing and activism around environmental racism issues, including air pollution and asthma, for example, in the South Bronx, West Harlem, and Ironbound.[8-10] Air quality can vary substantially between neighborhoods in the same city, and recent observational and computational advances have improved quantitative estimates of intraurban inequalities across the U.S.[11-17] However, fine-scale pollutant mapping typically relies on measurements that are short timescale snapshots or long time averages, trading temporal information for enhanced spatial detail. As a result, we have less knowledge of temporal variability in neighborhood-level inequalities and relationships between inequalities, urban air quality issues such as ozone, and climate change.

Nitrogen dioxide (NO_2) is a criteria pollutant and surface ozone (O_3) precursor. NO_2 is a chemically reactive primary pollutant, and, therefore, NO_2 concentrations are variable in space and time, with characteristic NO_2 distance decay gradients away from sources equaling hundreds of meters to 2 km.[18-20] NO_2 is emitted as NO_x ($\equiv NO + NO_2$), with sources dominated by fossil fuel combustion in cities, especially traffic exhaust.[21-23] NO_2 exposure is associated with numerous adverse health effects,[24-29] and roadway residential proximity has been linked to asthma-related urgent medical visits, pediatric asthma, cardiac and pulmonary mortality, and preeclampsia and preterm birth.[30-35] NO_2 concentrations and NO_x sources are unequally distributed with race, ethnicity, and income in U.S. cities,[1, 2, 4-6, 12-14, 17, 36] with urban NO_2 inequalities being large enough to cause health disparities.[11, 24]

To date, air pollution inequality analyses focusing on primary pollutants like NO_2 have typically prioritized spatial rather than temporal information, as observations and models must resolve length scales of atmospheric dispersion to fully describe disparities. Satellite NO_2 tropospheric vertical column densities (TVCDs) have been incorporated into regression models and other measurement-model hybrid surface NO_2 products relevant for health and environmental justice applications, with spatial resolutions ranging 100 m to 0.01° (~1 km).[11, 12, 24] The TROPOspheric Monitoring Instrument (TROPOMI) currently provides the highest spatial resolution global satellite NO_2 TVCDs, with TROPOMI describing NO_2 inequalities at census tract scales directly after TVCDs are oversampled to 0.01° x 0.01°, time averaging at least multiple months of measurements.[13, 14, 17] For reference, the average area of census tracts in New York City and Newark is 2.1 km^2. Oversampled TVCDs have been shown to observe NO_2 inequalities equivalently to high spatial resolution (250 m x 500 m) airborne remote sensing to within associated uncertainties, independently of patterns in the structure and heterogeneity of urban racial segregation, and similarly as measured at the surface.[13, 17] TROPOMI has an order of magnitude improved spatial resolution than its predecessor OMI, enabling analyses of NO_2 spatial distributions with less time averaging,[37, 38] potentially revealing new insight into the sources and controls over intraurban NO_2 inequalities. However, with current TROPOMI nadir pixel areas of ~20 km^2, the need for oversampling is assumed. As a consequence of the loss in temporal resolution, distributive NO_2 inequalities are not easily situated within our broader understanding of urban air quality and climate, and vice versa.

In this manuscript, we evaluate the use of daily TROPOMI observations to describe census tract-scale NO_2 inequalities with race, ethnicity, and income in the New York City–Newark urbanized area (UA). First, we report NO_2 inequalities using airborne remote sensing capable of resolving NO_2 distance decay gradients, with pixel dimensions of 250 m x 250 m, collected during the 2018 NASA Long Island Sound Tropospheric Ozone Study (LISTOS). The airborne observations serve as a reference for evaluating tract-scale NO_2 inequalities determined using spatially and temporally coincident daily TROPOMI NO_2 TVCDs. We show that the airborne and TROPOMI inequalities are strongly correlated and the daily TROPOMI TVCDs resolve a major portion of tract-scale NO_2 inequalities. We calculate daily TROPOMI NO_2 inequalities from May 2018–September 2021 and analyze biases in individual and mean daily TROPOMI results as a function of measurement pixel area, which range 20 to 91 km^2, and UA sampling coverage. Finally, we interpret empirical relationships between daily TROPOMI NO_2 inequalities and overall NO_2 pollution, O_3 air quality, and climate-relevant atmospheric conditions.

2 MEASUREMENTS AND METHODS

GCAS and GeoTASO. The Geostationary Coastal and Air Pollution Events (GEO-CAPE) Airborne Simulator (GCAS)[39] and Geostationary Trace gas and Aerosol Sensor Optimization (GeoTASO)[40] instruments are push broom spectrometers that function as satellite analogs for

NASA airborne missions. GeoTASO makes hyperspectral nadir-looking measurements of backscattered solar radiation in the ultraviolet (290–390 nm) and visible (415–695 nm). GCAS makes similar observations at 300–490 nm (optimized for air quality) and 480–900 nm (optimized for ocean color). Each of the two channels in both instruments use two-dimensional charge-coupled device (CCD) array detectors, where one CCD dimension provides the spectral coverage, one provides the cross-track coverage across a 45° field of view, and the movement of host aircraft generates the along-track coverage. The GCAS and GeoTASO datasets used here have identical NO_2 retrieval algorithms, which are similar to those of major satellite instruments, including TROPOMI, and eventually TEMPO.[41-43] Briefly, NO_2 differential slant columns are produced by fitting the 425–460 nm spectral window using QDOAS and a measured reference spectrum collected over a nearby area away from NO_2 sources. Differential slant columns are converted to vertical column densities using an air mass factor (AMF), which is a function of viewing and solar geometries, surface reflectance, and meteorological and trace-gas vertical profile shapes, among other variables (see Judd et al.[43] and Judd et al.[44] for details). NO_2 vertical profiles are calculated using bias-corrected PRATMO stratospheric NO_2 climatologies[41, 45, 46] and hourly output from the North American Model-Community Multiscale Air Quality (NAMCMAQ) model (12 km x 12 km) from a developmental analysis from the National Air Quality Forecasting Capability.[47] The resulting GCAS and GeoTASO TVCDs have a spatial resolution of 250 m x 250 m.

During the Long Island Sound Tropospheric Ozone Study (LISTOS), GeoTASO flew on the NASA LaRC HU-25 Falcon in June 2018 and GCAS flew onboard the NASA LaRC B200 from July–September 2018. On days when elevated regional air pollution was predicted (Table S1), a large raster flight pattern spanning nearly the full New York City–Newark UA (Figures 1a and S1a) was mapped in the morning (9–11 am local time, LT) and afternoon (1:30–4:10 pm LT). On other days, aircraft followed a smaller raster flight pattern (Figure S1b), sub-sampling the UA in the early morning (8:15–9:50 am LT), late morning (9:50–11:30 am LT), early afternoon (1:15–3:00 pm LT), and late afternoon (3:00–4:45 pm LT). During LISTOS, Judd et al.[44] reported GCAS and GeoTASO TVCDs agreed with coincident ground-based Pandora NO_2 column measurements to within ±25% with no apparent overall bias. Here, we focus on cloud-free observations from 37 large and small NO_2 TVCD flight rasters collected on 13 days having sampled at least 60% of census tracts in the New York City-Newark UA. On average, GCAS and GeoTASO sampled 79 ± 7% of UA census tracts. Compared to the full New York City-Newark UA, Black and African Americans, Hispanics and Latinos, and Asians were overrepresented by 16–25% in census tracts sampled during the large and especially small raster pattern (Table S2).

TROPOMI. The TROPospheric Ozone Monitoring Instrument (TROPOMI) is a hyperspectral spectrometer onboard the sun-synchronous Copernicus Sentinel-5 Precursor (S-5P) satellite.[48, 49] S-5P has an equatorial crossing time of 1:30 pm LT, with observations collected over the New York–Newark UA (Figure 1b) between 1–3 pm LT once or twice daily. NO_2 is retrieved by fitting the 405–465 nm spectral band based on an updated OMI DOMINO algorithm and work from the QA4ECV project.[50-54] NO_2 TVCDs have a documented low-bias over polluted scenes, with uncertainties driven by spatially and temporally coarse inputs to the AMF,[55] including the surface albedo (monthly 0.5° × 0.5° OMI climatology)[56] and NO_2 profile shape (daily 1° × 1° TM5-MP output).[57] We use Level 2 NO_2 TVCDs reprocessed on the S5P-PAL system (qa value > 0.75). From 1 May 2018 to 6 August 2019, encompassing the LISTOS period, the nadir spatial resolution of TROPOMI NO_2 TVCDs was 3.5 km x 7 km, with typical individual pixel areas of 27–63 km^2 (mean ± 1σ). Subsequently, the spatial resolution improved to 3.5 km x 5.5 km at nadir,[58] giving pixel areas of 21–49 km^2 (mean ± 1σ) over the New York City–Newark UA. We focus on the individual daily TVCDs (an example is shown in Figure 1b) and observations over May 2018–September 2021 oversampled to 0.01° x 0.01° using a physics-based algorithm (Figure 1c).[59]

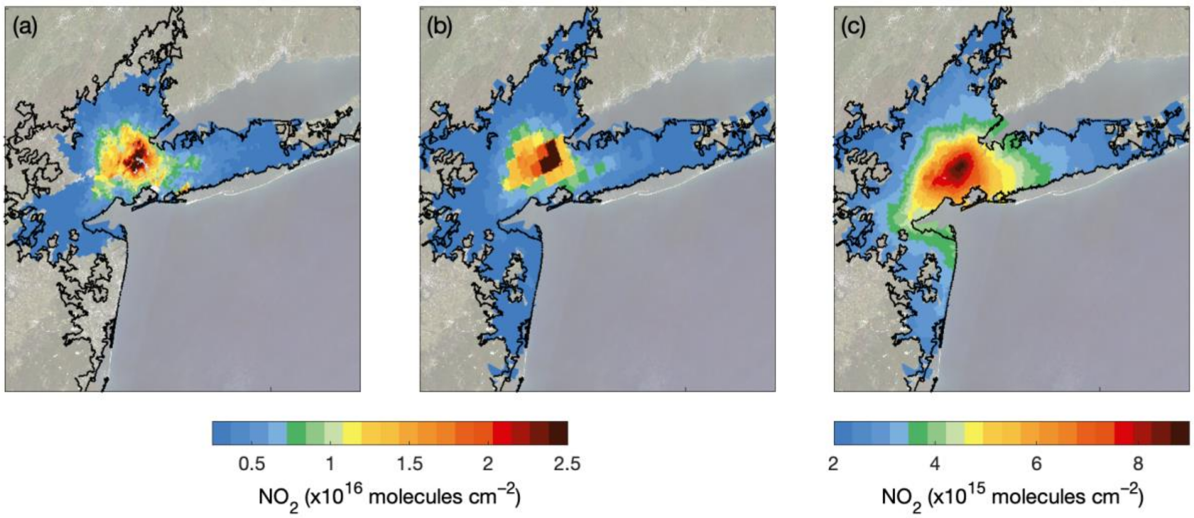

Figure 1. Example airborne NO_2 TVCDs (molecules cm^{-2}) collected on 30 June 2018 at 1–4 pm during a large raster flight pattern (250 m x 250 m) (a), TROPOMI measurements on the same day, which have a mean pixel area of 43 km^2 (b), and TROPOMI observations oversampled to 0.01° x 0.01° over 1 May 2018–30 September 2021 averaged to underlying census tracts. The black outline describes the New York City–Newark UA. Background map data: Landsat 8 composite January 2017–June 2020.

Census Tract NO_2 Inequalities. We average NO_2 TVCDs within 2018 census tract polygons for the New York City–Newark UA. Individual airborne and TROPOMI TVCDs are spatially continuous but discretized to 0.001° x 0.001° at the pixel level prior to tract averaging without regridding or oversampling. NO_2 tract-averaged TVCDs are weighted by tract-scale populations of non-Hispanic/Latino Black and African Americans, non-Hispanic/Latino Asians, all races identifying as Hispanic or Latino, and non-Hispanic/Latino whites (Eq. S1). Poverty status is defined according to the U.S. Census Bureau family Ratio of Income to Poverty. Poverty thresholds vary by family size and family member age but not geographically. The U.S. Census intends for poverty thresholds to be a "statistical yardstick" rather than a complete representation of families' needs. Below-poverty tracts are those with greater than 20% of households having an income-to-poverty ratio <1. Tracts above the poverty line are defined as those with household income-to-poverty ratios of >1. Tract-scale NO_2 TVCDs within both categories are population weighted by residents at the given poverty status. We combine race-ethnicity and income metrics, categorizing census tracts as low-income and non-white (LIN), i.e., people of color in low-income tracts, or high-income and white (HIW). In LIN tracts, NO_2 TVCDs are weighted by the population of Black and African Americans, Hispanics and Latinos, Asians, and/or American Indians and Alaska Natives in the lowest income quintile tracts (household incomes <$49,544.50). Because American Indians and Alaska Natives comprise less than 0.2% of the New York City–Newark UA population, we do not report results for this group separately. In HIW tracts, TVCDs are weighted by the population of non-Hispanic/Latino whites in the highest income quintile tracts (household incomes >$117,664). When we compute results in New York City and Newark separately, dividing the UA along state lines, lowest income quintile tracts are those with tract-averaged median household incomes <$48,911 and <$51,250, respectively; highest income quintile tracts are those with tract-averaged median household incomes >$112,940 and >$125,367, respectively. We discuss NO_2 disparities in terms of relative and absolute inequalities computed as percent (%) and absolute differences (molecules cm^{-2}) in population-weighted census tract-averaged TVCDs. Race-ethnicity inequalities are in reference to population-weighted NO_2 TVCDs for non-Hispanic/Latino whites and poverty status inequalities are in reference to NO_2 TVCDs in census tracts above the poverty line. While there are numerous dimensions of air pollution inequity, our focus is on the evaluation and application of daily satellite measurements; therefore, we limit the number of demographic characteristics considered in the analysis. Census data are from the 2019 American Community Survey (ACS): 5-Year dataset. Fractional census tract populations for the four largest race-ethnicity groups and median household incomes are mapped in Figure 2 and census tract population densities are shown in Figure S2. The ACS is a higher time resolution alternative to the longform decennial census. The ACS accounts for variations in census tract sampling rates and differential group response rates through a complex weighting process. Sample weights prioritize accuracy over precision, with individual tract estimates being more imprecise in tracts with heterogeneous populations.[60, 61] We manage this imprecision through aggregation by population weighting. We focus on the UA, defined as densely populated and commercial areas within cities, to describe intraurban inequalities rather than urban-suburban differences.

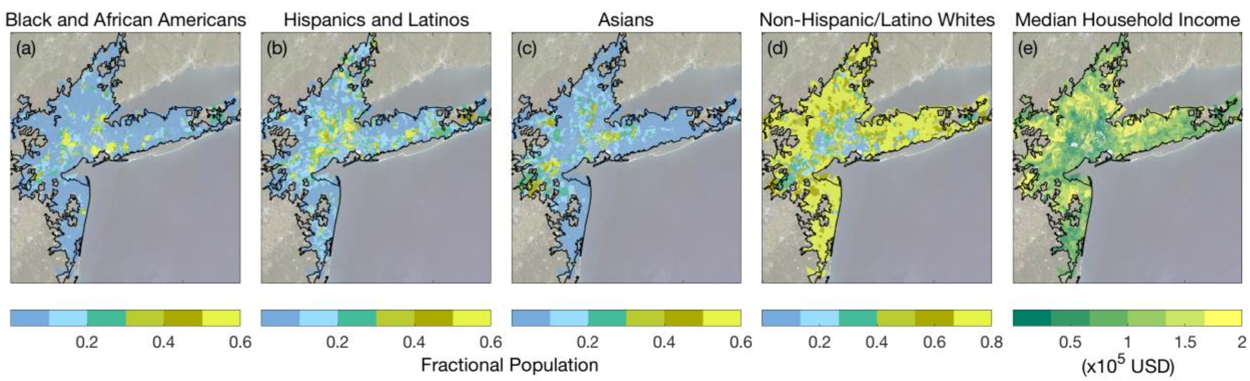

Figure 2. Fractional census tract populations for Black and African Americans (a), Hispanics and Latinos of all races (b), Asians (c), non-Hispanic/Latino whites (d), and median household incomes (e) in the New York City–Newark UA (black line). Background map data: Landsat 8 composite January 2017–June 2020.

Measurements of Surface NO_2*, O_3, and Meteorology. We use NO_2* surface observations collected at 11 stations across the New York City–Newark UA (Figure S3a). These measurements are made by decomposing NO_2 to NO over a heated molybdenum catalyst, followed by the detection of NO using the chemiluminescence technique. The resulting NO_2 data have a known positive interference from higher-order nitrogen oxides and ammonia, which also decompose at non-unity efficiency in the presence of the catalyst.[62-64] We use the term NO_2* in acknowledgement of this interference, opting not to apply a correction factor as we are interested in the distance dependence of the correlations between surface NO_2* and overhead TVCDs, rather than the surface NO_2 mixing ratios themselves. We use O_3 measurements from 17 monitoring stations within the UA (Figure S3b) converted to the policy-relevant metric of the daily maximum 8-hour average (MDA8) O_3 mixing ratio. Temperature and wind speed measurements are collected at 14 stations throughout the New York City–Newark UA as part of the Automated Surface Observing System and Automated Weather Observing System (Figure S3c), accessible through the Iowa State University Iowa Environmental Mesonet download service. Because of station-level variability in the data collection interval, we average individual station meteorological measurements from 12–3 pm local time (LT) prior to computing the UA-wide mean.

NO_x Emissions Inventories: FIVE and NEI. The Fuel-based Inventory of Vehicle Emissions (FIVE) tabulates monthly on-road and off-road gasoline and diesel mobile source emissions at 4 km x 4 km U.S. wide. The FIVE is based on publicly available datasets of taxable fuel sales and road-level traffic and time-resolved weigh-in-motion traffic counts.[22, 65, 66] We use emissions from the 2018, 2019, 2020 COVID-19, and 2020 business-as-usual (BAU) FIVE for 2018, 2019, 2020, and 2021, respectively. The 2020 COVID-19 inventory was developed using monthly scaling factors from U.S. Energy Information Administration fuel sales reports.[22] In the 2020 BAU FIVE, fuel use is assumed unchanged from 2019.[22] See McDonald et al.[65] and Harkins et al.[22] for a detailed discussion of the uncertainties, which are ±24% for both gasoline and diesel vehicles. Annual NO_x stationary source emissions are taken from the 2017 National Emissions Inventory (NEI17), including industrial and commercial facilities, power plants, and airports. Uncertainties in power plant emissions are ±25% and uncertainties for industrial facilities and other stationary sources are ±50%.[67, 68]

3 RESULTS AND DISCUSSION

GCAS and GeoTASO Census Tract-Level NO_2 Inequalities during LISTOS. We report population-weighted census tract-scale NO_2 inequalities measured during each of the 37 LISTOS flights within the New York City–Newark UA in Figure 3 and Table S3. Population-weighted NO_2 TVCDs for Black and African Americans, Hispanics and Latinos, and Asians are 14 ± 3%, 14 ± 5%, and 15 ± 4% higher than for non-Hispanic/Latino whites, respectively. NO_2 TVCDs are on average 17 ± 4% greater in tracts below the poverty line compared to those above. When race-ethnicity and income metrics are combined, NO_2 TVCDs are 24 ± 4% higher in LIN than HIW census tracts. Errors are defined as 95% confidence intervals for mean inequalities, derived from bootstrapped distributions sampled with replacement 10^4 times.

NO_2 inequalities are more variable between days than by time of daytime during LISTOS. While population-weighted and/or income-sorted NO_2 TVCDs for all groups are on average 14–28% higher during morning (8–11:30 am LT) than afternoon flights (1–5 pm LT), corresponding median relative and absolute NO_2 inequalities are not significantly different for any group (Mann-Whitney test, $p < 0.050$). Mean relative and absolute inequalities are also similar during morning and afternoon flights, with exceptions of relative inequalities for Hispanics and Latinos and absolute inequalities for Asians and in LIN tracts. This suggests observations collected in the early afternoon by TROPOMI capture daytime patterns in tract-scale population-weighted NO_2 TVCD (not surface mixing ratio) differences generally, at least during LISTOS. The small number of flights limits our ability to statistically infer relationships between NO_2 disparities and environmental factors; however, we observe moderate, negative correlations between absolute inequalities and mean surface wind speeds and moderate, positive correlations with UA-mean NO_2* and NO_2 TVCDs for some groups ($p < 0.050$) (Table S4). This is consistent with slower surface winds reducing the mixing of NO_2 pollution away from NO_x sources and higher NO_2 pollution worsening absolute inequalities.

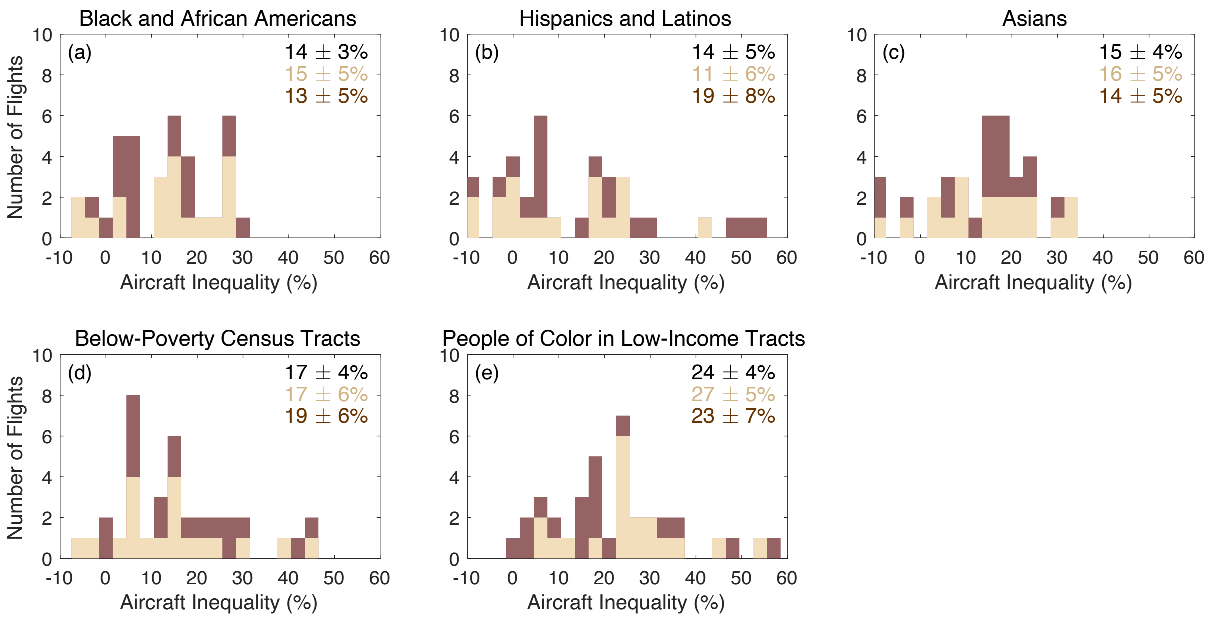

Figure 3. Airborne NO_2 inequalities for each of the 37 LISTOS flights for Black and African Americans (a), Hispanics and Latinos (b), and Asians (c) compared to non-Hispanic/Latino whites, below poverty versus above poverty tracts (d), and LIN compared to HIW tracts (e). Morning (8–11:30 am LT) (tan) and afternoon (1–5 pm LT) (brown) flights are shown separately. LISTOS mean inequalities with 95% confidence intervals are reported in each panel, for all flights (black) and separately in the morning (tan) and afternoon (brown).

Evaluating Daily TROPOMI Observations. To determine the extent to which daily TROPOMI measurements resolve census tract-level disparities, we compare NO_2 inequalities for spatially and temporally coincident tract-averaged GCAS, GeoTASO, and TROPOMI observations within the New York City–Newark UA. We consider measurements to be coincidental if the minimum and maximum overfly times of airborne columns within a given census tract occur within ±30 minutes of the TROPOMI overpass. Daily relationships between airborne and TROPOMI inequalities are fit using an unweighted bivariate linear regression model (Figure 4).[69] We infer the portion of NO_2

inequalities captured by TROPOMI from the slope of this line and assess agreement between the airborne and TROPOMI-derived results using Pearson correlation coefficients.

Daily TROPOMI observations capture most tract-scale NO_2 differences and are well correlated with inequalities measured by GCAS and GeoTASO. Correlation slopes are 0.82 ± 0.10–1.05 ± 0.07 for relative inequalities and 0.76 ± 0.09–0.96 ± 0.06 for absolute inequalities, implying TROPOMI detects at least 82% of relative and 76% of absolute inequalities, with slopes for many population groups being even higher. For the comparison, the mean pixel area of coincident TROPOMI TVCDs is 44 ± 18 km^2 (±1σ), which is much larger than typical atmospheric NO_2 distance decay gradients of a few hundred meters.[18-20] While some precision is lost, our results suggest measurements on the scale of these gradients, for example GCAS and GeoTASO, are not required to constrain the majority of city-wide census tract-scale NO_2 inequalities. Airborne and TROPOMI inequalities are strongly correlated, with Pearson correlation coefficients ranging 0.82–0.97 for relative and 0.88–0.96 for absolute inequalities. Slopes and Pearson correlation coefficients do not improve significantly when inequalities are weighted by the number of coincident census tracts, mean TROPOMI pixel areas, UA-mean surface wind speeds, or mean TROPOMI NO_2 TVCDs, suggesting these variables do not have a strong influence over the agreement, at least in the New York City–Newark UA during LISTOS.

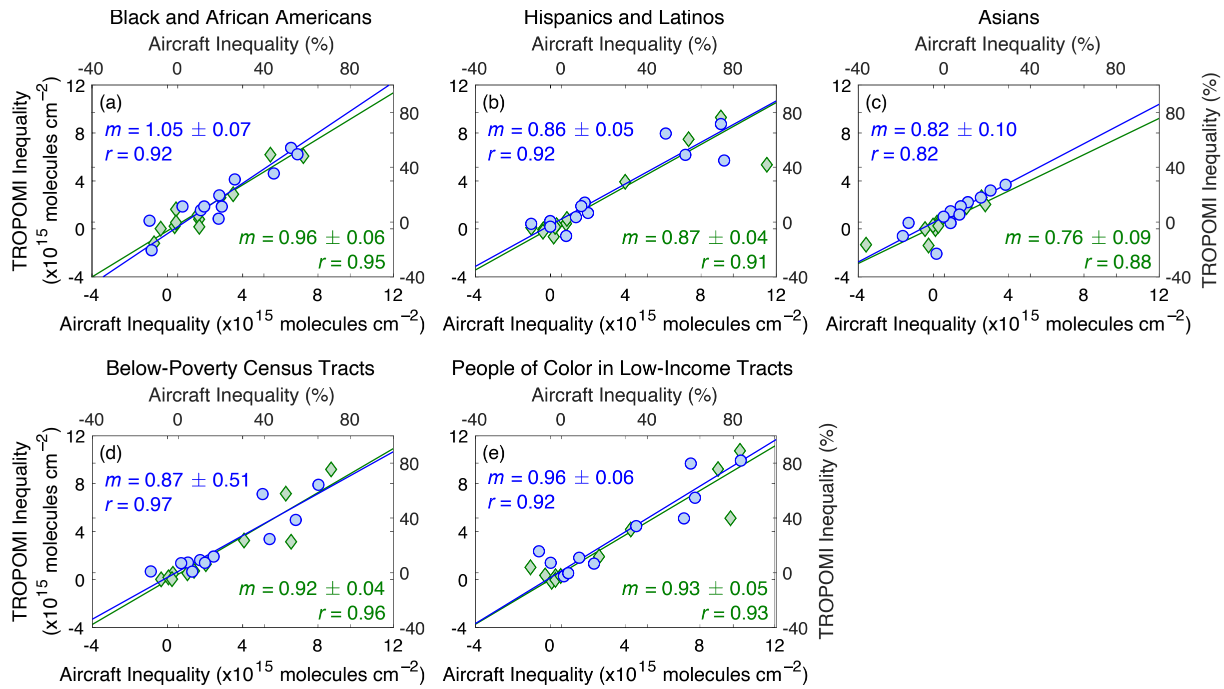

Figure 4. Daily relative (%) (blue circles) and absolute (molecules cm^{-2}) (green diamonds) inequalities measured by GCAS and GeoTASO versus TROPOMI during LISTOS for Black and African Americans (a), Hispanics and Latinos (b), and Asians (c) compared to non-Hispanic/Latino whites, below-poverty versus above poverty tracts (d), and LIN compared to HIW tracts (e). Fits are derived from an unweighted bivariate linear regression model. Slopes (*m*) and Pearson correlation coefficients (*r*) for each fit are reported for both relative (blue) and absolute (green) inequalities. One data point in panel d is out of frame (–119.5, –136.4).

Table 1. Influence of TROPOMI pixel area and sampling coverage on both mean and individual daily relative inequalities (May 2018–September 2021), as well as comparison between mean daily and oversampled relative inequalities for Black and African Americans, Hispanics and Latinos, and Asians compared to non-Hispanic/Latino whites, for below poverty versus above poverty tracts, and for LIN compared to HIW tracts. The pixel area analysis only includes days with >30% UA coverage. Observations are grouped such that each category contains at least 80 observation days. Inequalities are binned by days with low (<30%), moderate (30–60%), and high (>60%) UA coverage. Daily inequalities are assessed using the coefficient of variation. Errors are 95% confidence intervals based on bootstrapped distributions sampled with replacement 10^4 times. The oversampled TROPOMI TVCDs are oversampled to 0.01° x 0.01° prior to census tract averaging for all days, on days with >30% coverage, and on days with >60% coverage, with uncertainties as standard mean errors.

	Mean of Daily Inequalities					**Daily Inequalities**				
	Relative Inequalities (%)					**Coefficient of Variation**				
Pixel Area (km^2)	Black and African Americans	Hispanics and Latinos	Asians	Below Poverty Tracts	LINs	Black and African Americans	Hispanics and Latinos	Asians	Below Poverty Tracts	LINs
20–25	31 ± 2	30 ± 2	28 ± 2	28 ± 2	40 ± 3	0.44	0.52	0.43	0.45	0.40
25–30	32 ± 3	30 ± 3	28 ± 2	26 ± 3	39 ± 3	0.45	0.53	0.42	0.52	0.41
30–35	31 ± 3	29 ± 3	30 ± 2	26 ± 2	38 ± 3	0.42	0.42	0.32	0.43	0.37
35–45	31 ± 2	26 ± 3	28 ± 2	25 ± 3	38 ± 3	0.37	0.62	0.34	0.53	0.41
45–60	30 ± 3	27 ± 3	28 ± 3	25 ± 2	38 ± 4	0.54	0.60	0.51	0.53	0.53
>60	26 ± 3	25 ± 3	23 ± 2	22 ± 2	31 ± 3	0.47	0.60	0.49	0.50	0.43
UA Coverage (%)										
<30	12 ± 2	11 ± 2	10 ± 2	11 ± 4	18 ± 4	1.99	2.00	2.05	2.47	1.81
30–60	30 ± 3	29 ± 3	26 ± 3	25 ± 3	37 ± 4	0.64	0.62	0.65	0.66	0.65
>60	30 ± 1	28 ± 1	28 ± 1	26 ± 1	38 ± 1	0.40	0.53	0.36	0.45	0.36
	Mean of Daily Inequalities					**Oversampled Inequalities**				
All days	24 ± 1	22 ± 1	21 ± 1	21 ± 1	32 ± 1	28 ± 1	27 ± 1	28 ± 1	25 ± 1	36 ± 2
>30%	30 ± 1	28 ± 1	28 ± 1	25 ± 1	38 ± 1	28 ± 1	27 ± 1	28 ± 1	25 ± 1	35 ± 2
>60%	30 ± 1	28 ± 1	28 ± 1	26 ± 1	38 ± 1	28 ± 1	26 ± 1	28 ± 1	25 ± 1	36 ± 2

We calculate daily census tract-scale NO_2 inequalities over May 2018–September 2021 and investigate the sensitivity of mean and individual daily results to UA-mean TROPOMI pixel area and UA coverage percentage (Table 1). First, UA-mean daily TROPOMI pixel areas range ~20–90 km^2 (Figure S4), providing an empirical test of the resolution dependence of NO_2 inequalities. We remove days from the analysis when TROPOMI observations cover less than 30% of census tracts across the New York City–Newark UA (justification below; see Table S5 for an analysis of all days). We find relative inequalities are mostly insensitive to TROPOMI UA-mean pixel area, with significant differences in medians emerging when pixels are larger than ~60 km^2, defined as $p < 0.050$ (Kruskal-Wallis test). Additionally, there is no clear influence of increasing UA-mean pixel area on the coefficient of variation of the individual daily inequalities. Substantial day-to-day variability limits our ability to identify an exact pixel area-sensitivity threshold, and, because observation days with UA-mean pixel areas >60 km^2 comprise less than 15% of the full dataset, their inclusion does not significantly affect our results. Relationships between inequalities and UA-mean pixel areas suggest key spatial scales for describing NO_2 inequalities are larger than those of atmospheric NO_2 dispersion gradients, which is consistent with recent work by Chambliss et al.[16] and Demetillo et al.[13], because NO_x emissions sources are ubiquitous and distributed and tracts with similar population characteristics spatially aggregate.[70]

Second, we investigate the sensitivity of daily inequalities to TROPOMI observation UA coverage extent (Table 1). Reduced sampling coverage is largely caused by clouds, but snow accumulation can be important in the winter. In the New York City–Newark UA, snow cover accounted for 29% of missing pixels in winter months, with snow present on 43% of observations days in December–February and 12% of total observation days across May 2018–September 2021. Distributions of daily relative and absolute NO_2 inequalities for each group are shown in Figure 5 on all days, on days with at least 30% UA coverage, and on days with at least 60% UA coverage. Inclusion of days with sparse coverage (<30%) decreases mean relative NO_2 inequalities by 4–6 percentage points. Individual daily inequalities are more affected by missing data than means, with increasing coefficients of variation at UA coverage levels of <60% in comparison to days with >90% coverage. Effects of incomplete UA coverage are largely explained by insufficient sampling of key race-ethnicity, poverty, and income groups, with greater coverage capturing more representative UA demographics and observations on lower coverage days more likely to sample population groups in the majority (Figure S5): non-Hispanic/Latino whites (44%) and tracts above the poverty line (73%). As a result, we remove days with <30% UA coverage from our discussion of mean NO_2 inequalities (323 days or 33% of the full dataset) and days with <60% coverage from our analysis of daily inequalities (457 days or 47% of the full dataset). Results are skewed toward clear sky conditions, corresponding to daytime (12–3 pm LT) mean surface NO_2* mixing ratios of 8.1 ± 4.4 ppb (days with >30% UA coverage) compared to daytime mean NO_2* of 11.9 ± 6.6 ppb (days with <30% coverage), likely biasing daily absolute NO_2 inequalities low (discussion below).

Mean daily population-weighted NO_2 TVCDs over May 2018–September 2021 are 30 ± 1%, 28 ± 1%, and 28 ± 1% higher for Black and African Americans, Hispanics and Latinos, and Asians, respectively, compared to non-Hispanic/Latino whites (Figure 5 and Table 1). NO_2 TVCDs are 25 ± 1% greater in tracts below the poverty line than above and 38 ± 1% higher in LIN compared to HIW census tracts. We report results separately in New York City and Newark, where mean daily NO_2 inequalities are 19–30% and 24–43%, respectively (Table 2). Means and 95% confidence intervals are derived from bootstrapped daily NO_2 inequality distributions resampled 10^4 times. We repeat NO_2 inequality calculations by first oversampling the same subset of days to a resolution of 0.01° x 0.01° using a physics-based algorithm[59] prior to census tract averaging and find oversampled and mean daily results are equal to within associated uncertainties for days with at least 30% UA coverage (Table 1). Finally, our analysis is based on recently reprocessed S5P-PAL TROPOMI TVCDs, which include improvements resolving some of the low biases occurring over polluted northern midlatitude scenes and in the wintertime.[71] Mean daily inequalities computed with the S5P-PAL TVCDs are 3–6 percentage points higher compared to the RPRO and OFFL operational products (Table 2), indicating TROPOMI NO_2 inequality estimates using previously available NO_2 products are biased low, as suggested by Demetillo et al.[17] in their detailed evaluation of oversampled NO_2 TVCDs and census tract-scale inequalities in Houston, Texas.

While inequalities based on spatially and temporally coincident airborne and TROPOMI TVCDs are in good agreement (Figure 4), mean daily TROPOMI NO_2 inequalities are significantly higher than those measured by GCAS and GeoTASO during LISTOS (Table 1). This is true both over the full May 2018–September 2021 period and on LISTOS flight days when all TROPOMI TVCDs, not just those coincident with airborne observations, are considered. Absolute inequalities are higher in the winter than summer; however, relative NO_2 inequalities exhibit little seasonal variation. While LISTOS inequalities are within the distribution of daily TROPOMI inequalities, differences in mean disparities are explained by changes in UA observational coverage and corresponding demographic composition. Mean daily TROPOMI inequalities within a typical LISTOS large (30 June 2018) and small (15 August 2018) flight raster are 3–9 and 11–20 percentage points lower than across the full New York City–Newark UA (Table 2). However, there are similarities, for example, mean inequalities for Black and African Americans, Hispanics and Latinos, and Asians are comparable to within associated uncertainties, as also observed by GCAS and GeoTASO during LISTOS, and inequality distributions for Hispanics and Latinos exhibit a heavy tail using both daily TROPOMI and aircraft TVCDs.

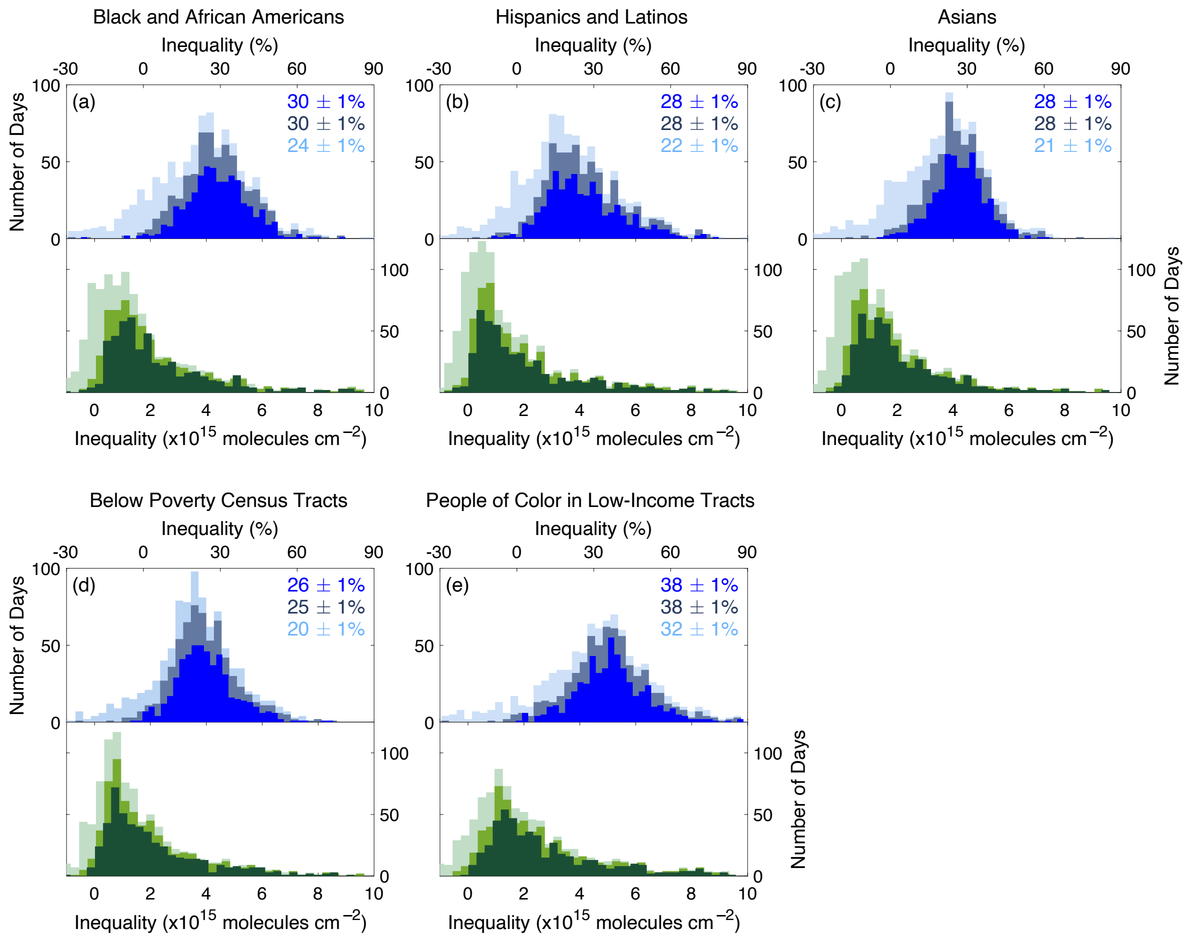

Figure 5. Daily TROPOMI NO_2 inequalities over May 2018–September 2021 for Black and African Americans (a), Hispanics and Latinos (b), and Asians (c) compared to non-Hispanic/Latino whites, below-poverty versus above poverty tracts (d), and LIN compared to HIW tracts (e). Top panels depict relative inequalities (%) on all days (light blue), on days with at least 30% UA coverage (gray blue), and on days with at least 60% UA coverage (bright blue). Bottom panels depict absolute inequalities (molecules cm^{-2}) on all days (light green), days with at least 30% UA coverage (yellow green), and on days with at least 60% UA coverage (dark green). Mean relative inequalities and 95% confidence interval are included in each panel for each coverage threshold: on all days (light blue), on days with at least 30% UA coverage (gray blue), and on days with at least 60% UA coverage (bright blue).

Table 2. Mean daily TROPOMI inequalities (May 2018–September 2021) on days with >30% coverage across the New York City–Newark UA based on the S5P-PAL NO_2 product, as used throughout the analysis, on days with >30% coverage based on the RPRO and OFFL operational products, separately in New York City and Newark, and within the large (30 June) and small (15 August) LISTOS flight rasters. Errors are 95% confidence intervals based on bootstrapped distributions sampled with replacement 10^4 times.

	New York City–Newark UA (S5P-PAL)	New York City–Newark UA (Operational Product)	New York City, NY	Newark, NJ	Large LISTOS Raster Flight Pattern	Small LISTOS Raster Flight Pattern
Black and African Americans	30 ± 1	26 ± 1	22 ± 1	33 ± 2	22 ± 1	10 ± 1
Hispanics and Latinos	28 ± 1	23 ± 1	19 ± 1	43 ± 2	20 ± 1	11 ± 1
Asians	28 ± 1	25 ± 1	25 ± 1	26 ± 2	19 ± 1	10 ± 1
Below Poverty Tracts	25 ± 1	22 ± 1	20 ± 1	24 ± 1	22 ± 1	14 ± 1
LINs	38 ± 1	32 ± 1	30 ± 1	43 ± 1	32 ± 1	20 ± 1

Finally, TROPOMI measures NO_2 atmospheric columns rather than surface mixing ratios. For satellite remote sensing to inform environmental justice decision-making, spatial and temporal patterns in TVCDs must reflect NO_2 distributions at the surface.[13, 17] To investigate NO_2 column-surface relationships, we calculate Pearson correlation coefficients between daily TROPOMI TVCDs (without averaging to underlying census tracts) and mean daytime (12–3 pm LT) NO_2* mixing ratios as a function of the distance between observations.[13, 17, 72] We find the strongest mean correlations (r = 0.61 ± 0.03; error is the 95% confidence interval) between NO_2* and directly overhead TVCDs, defined as TVCDs within 1 km of a monitor based on pixel center points. Mean daily column-surface correlations subsequently weaken with increasing distance, falling to 0.56 ± 0.03 at 1–2 km, 0.49 ± 0.02 for 2–5 km, and 0.43 ± 0.02 at 5–10 km. The distance dependance of mean Pearson correlation coefficients reflects typical NO_2 distance decay gradients,[18-20] indicating coarser resolution daily observations resolve finer-scale NO_2 gradients, at least to some extent in the average. Column-surface correlations covary with wind speeds and overall NO_2 pollution levels in physically meaningfully ways. Daily r values are significantly, although weakly, negatively associated with UA-mean surface wind speeds and positively associated with UA-mean NO_2* and NO_2 TVCDs. Lastly, we find no relationship between Pearson column-surface correlation coefficients and daily UA-mean pixel area (Table S6).

Daily Variability in NO_2 Inequalities. Here, we apply the daily TROPOMI NO_2 inequality observations, describing statistical relationships with overall NO_2 and O_3 pollution and climate-relevant atmospheric conditions (Table 3). We discuss the implications of each in turn. We report Pearson correlation coefficients between NO_2 inequalities, surface NO_2* mixing ratios, and NO_2 TVCDs. We compute Spearman rank correlation coefficients (ρ) between NO_2 inequalities, MDA8 O_3, surface wind speeds, and surface daytime and daily maximum temperatures, as these relationships are monotonic but nonlinear. Surface NO_2* mixing ratios, wind speeds, and temperatures are UA-wide means over 12–3 pm LT in correspondence to the TROPOMI overpass time. We calculate r and ρ values on days with >60% TROPOMI UA coverage, separately in the winter (December–February) and summer (June–August).

First, we find absolute NO_2 inequalities are strongly associated with UA-mean surface NO_2* and NO_2 TVCDs. However, relative inequalities are mostly uncorrelated in the winter and only weakly or moderately associated with NO_2 pollution in the summer. Observed differences between absolute and relative inequalities are evidence that NO_x sources are systematically located in communities of color and low-income neighborhoods, as variability in individual terms affecting the NO_2 mass balance will have a larger effect on absolute NO_2 concentrations than on relative differences city wide. Therefore, while incremental NO_x controls will decrease localized NO_2 burdens, any emissions above zero will drive continued disparities. Results from daily TROPOMI TVCDs are supported by predictions from the FIVE and NEI. We calculate inequalities in NO_x source densities equivalently to those based on observations (Methods), with point source emissions summed within census tracts and total NO_x emissions (FIVE + NEI) divided by tract area. Inequalities in population-weighted NO_x emission source densities are 90 ± 6% for Black and African Americans, 95 ± 5% for Hispanics and Latinos, 71 ± 6% for Asians, 88 ± 5% for below-poverty tracts, and 113 ± 7% for LINs.

NO_2 is a key reactant in the chemistry of O_3 production (PO_3); therefore, neighborhood-level NO_2 inequalities and urban O_3 are potentially coupled. In the New York City–Newark UA, there were 59 exceedances of the MDA8 70 ppb National Ambient Air Quality Standard (NAAQS) over May 2018–September 2021. Briefly, PO_3 is a nonlinear function of NO_2. At low NO_2 levels, NO_x emissions reductions decrease PO_3 (chemistry is NO_x limited). At high NO_2 levels, NO_x reductions increase PO_3 (chemistry is NO_x suppressed), with decreases in gas-phase organic compounds being the most effective form of O_3 control, at least until NO_2 is sufficiently reduced to transition to NO_x-limited PO_3. Here, we find absolute NO_2 inequalities are moderately, positively associated with summertime UA-mean MDA8 O_3 (Table 3), with similar results over the May–September O_3 season (Table S7). For comparison, correlation coefficients relating UA-mean surface NO_2* and column NO_2 TVCDs with MDA8 O_3 on >60% UA coverage days are 0.43 and 0.46, respectively. This suggests there are regulatory O_3 co-benefits to reducing NO_2 inequalities and to strategies prioritizing NO_x emissions reductions in communities of color and low-income communities, consistent with recent work showing PO_3 in New York City and Newark trending toward NO_x-limitation.[73] Because O_3 is an intermediately long-lived secondary pollutant, it is more evenly distributed and not generally associated with large intraurban exposure disparities.[74] However, NO_2 concentrations are highly spatially heterogeneous, and NO_2 reductions in neighborhoods overburdened by NO_x sources could potentially worsen O_3 locally. To investigate this, we compare population-weighted census tract-scale MDA8 O_3 NAAQS exceedance frequencies on weekdays and weekends based on surface O_3 measurements (Table S8). In the New York City–Newark UA, NO_2 TVCDs were on average 27% lower on weekends compared to weekdays over May 2018–September 2021. Across U.S. cities, weekday-weekend O_3 differences are a well-established test of the NO_2 dependence of PO_3, as substantial NO_2 decreases occur without comparatively large changes in other aspects of O_3 chemistry.[75] We find MDA8 O_3 NAAQS exceedances are more frequent on weekdays than weekends for all race, ethnicity, and/or income population groups (Table S8), indicating that NO_x reductions will not worsen O_3 where NO_x emissions are greatest. This said, we add caution that our results may be influenced by the locations of the O_3 monitors.

Finally, atmospheric conditions influence intraurban NO_2 distributions in ways that inform how NO_2 inequalities may scale with climate change. The Northeast U.S. is expected to experience warmer surface temperatures and more frequent stagnation days in summer and winter months, with slower surface winds from reduced mid-latitude cyclone activity and a northward shift of the summer mid-latitude jet stream.[76-81] We find NO_2 inequalities exhibit moderate to strong negative associations with surface wind speeds, consistent with the accumulation of NO_2 pollution near NO_x sources from reduced atmospheric mixing. This indicates that more frequent atmospheric stagnation events will exacerbate disparities. During summer months, NO_2 inequalities are weakly but significantly positively correlated with both daytime average and maximum daily temperatures. As a result, NO_2 inequalities and temperature may not scale together; however, people of color and low-income residents in New York City and Newark also bear disproportionate urban heat risks compared to non-Hispanic/Latino white and wealthy residents,[82-84] suggesting cumulative unequal climate-driven burdens will be greater without targeted NO_x emission controls.

Table 3. Correlation coefficients between daily absolute inequalities and UA-mean NO_2* mixing ratios (12–3 pm LT), NO_2 TVCDs, surface wind speeds (12–3 pm LT), surface temperatures (12–3 pm LT), daily maximum temperatures, and MDA8 O_3 mixing ratios. Relationships between daily NO_2 inequalities, surface NO_2*, and NO_2 TVCDs are Pearson correlation coefficients (r). All other relationships are Spearman rank correlation coefficients (ρ). Correlations are separately analyzed in the winter (December–February) and summer (June–August) for days with TROPOMI observations with >60% UA coverage. Only statistically significant coefficients are reported, with r and ρ significant to 1% ($p < 0.010$) unless indicated (†), which means significant to 5%.

	Correlations with Absolute Daily Inequalities						Correlations with Relative Daily Inequalities	
Summer								
	Surface Wind Speeds	Surface NO_2*	NO_2 TVCDs	MDA8 O_3	Surface Temperatures	Daily Maximum Temperature	Surface NO_2*	NO_2 TVCDs
Black and African Americans	–0.31	0.56	0.61	0.41	0.19†	0.19†	0.25	0.17†
Hispanics and Latinos	–0.24	0.62	0.67	0.55	0.28	0.33	0.46	0.39
Asians	–0.34	0.59	0.68	0.51	0.30	0.28	0.32	0.25
Below Poverty Tracts	–0.29	0.62	0.64	0.50	0.26	0.30	0.38	0.25
LINs	–0.32	0.63	0.66	0.50	0.23	0.27	0.40	0.24

	Correlations with Absolute Daily Inequalities				Correlations with Relative Daily Inequalities	
Winter						
	Surface Wind Speeds	Surface NO_2*	NO_2 TVCDs	Surface Temperatures	Surface NO_2*	NO_2 TVCDs
Black and African Americans	–0.75	0.60	0.65	–	–	–
Hispanics and Latinos	–0.65	0.70	0.64	–	0.44	0.28
Asians	–0.77	0.69	0.75	–	–	–
Below Poverty Tracts	–0.71	0.63	0.54	–	–	–
LINs	–0.78	0.64	0.60	–	–	–

Summary, Future Opportunities, and Implications. We have demonstrated that individual daily TROPOMI observations capture a major portion of census-tract scale NO_2 inequalities in the New York City–Newark UA using high spatial resolution (250 m x 250 m) GCAS and GeoTASO remote sensing measurements as a standard of comparison. LISTOS airborne observations resolve length scales of dispersion, allowing for accurate representations of tract averaged NO_2 TVCDs. We show that spatially and temporally coincident TROPOMI and aircraft measurements are strongly correlated (0.82–0.97) with slopes of 0.82 ± 0.10–1.05 ± 0.07 and 0.76 ± 0.09–0.96 ± 0.06 for relative and absolute inequalities, respectively. Moreover, daily TROPOMI NO_2 inequalities are generally insensitive to observation resolution for UA-mean pixel areas smaller than 60 km^2—therefore, key spatial scales for measuring NO_2 inequalities are larger than those of atmospheric NO_2 gradients,[16] as tracts with similar population characteristics spatially aggregate, even in New York City and Newark where the structure of racial segregation is highly heterogeneous.[13, 70] As a result, fine-scale observations may not always be required to understand variability in intraurban air pollution disparities, especially if biases can be well characterized, opening new opportunities for satellite remote sensing, as well as chemical transport modeling. We limit our conclusions to decision-making on city-wide NO_2 inequalities, as we have not attempted to resolve near-field impacts of individual polluters in communities with air pollution-related environmental justice concerns, instead focusing on accumulated NO_2 burdens from ubiquitous and overlapping urban NO_x sources. Daily TROPOMI observations cannot replace hyper-localized community-driven monitoring,[85] but spatially comprehensive and temporally resolved satellite measurements offer complimentary information on spatiotemporal trends and in unmonitored locations.

We report mean daily NO_2 inequalities of 28–30% for Black and African Americans, Hispanics and Latinos, and Asians and inequalities of 25% for residents of below poverty census tracts. When race-ethnicity and income metrics are combined, we find 38% greater population-weighted NO_2 TVCDs for people of color living in low-income tracts (LINs). These mean daily NO_2 inequalities equal those based on TROPOMI NO_2 TVCDs first oversampled to 0.01^o x 0.01^o to within associated uncertainties. Biases arise using individual observations with reduced UA coverage due to inadequate sampling of key race-ethnicity and income groups, affecting mean daily NO_2 inequalities and the precision of individual daily results (Figure S5). The dependence of city-level inequalities on sampling coverage has relevance for other measurement approaches for which it is difficult to collect observations city wide, for example, mobile monitoring. Reliance on clear sky measurements likely biases absolute NO_2 inequalities low, and relative inequalities to a smaller extent, as UA-wide mean surface NO_2* mixing ratios are 40% higher (3.8 ppb) on low (<30%) than high-coverage (>30%) days and as TROPOMI absolute inequalities are strongly, positively associated with overall NO_2 pollution, at least in the New York City–Newark UA.

Observations of daily NO_2 inequalities offer new insight into the causes and countermeasures of neighborhood-level disparities through their statistical relationships with other factors. We present empirical evidence for the systematic placement of NO_x sources in communities of color and low-income neighborhoods across the New York City–Newark UA. Specifically, absolute NO_2 inequalities are strongly correlated with overall NO_2 pollution, while relative NO_2 inequalities are not. The issue of source placement has been long identified by community organizations and residents, with TROPOMI providing space-based accountability of whether the promises of recent legislation in both states to consider cumulative burdens during permitting are kept.[86, 87] Municipalities have several tools for addressing existing siting disparities: establishing penalties; eliminating nonconforming uses; using environmental reviews, impact analyses, and comprehensive planning; and tightening existing zoning codes in polluted neighborhoods with marginalized and vulnerable populations. Daily TROPOMI observations enable approaches to prioritize affected communities where and when NO_2 burdens are highest. We find more frequent stagnation conditions in the coming decades will exacerbate neighborhood-level NO_2 inequalities, and warming summer surface temperatures will increase cumulative disparities from overlapping NO_2 and urban heat burdens. So informed, municipalities have opportunities for targeted interventions focused on redressing harms and eliminating disparities by preventing the arrival of new sources and decreasing existing NO_x emissions in overburdened communities. In addition, because NO_2 inequalities are positively associated with high MDA8 O_3 in the New York City–Newark UA, targeted NO_x emissions reductions in communities of color and low-income neighborhoods have the potential to improve O_3 city wide.

Acknowledgments. This research was funded by the NASA New (Early Career) Investigator Program in Earth Science (80NSSC21K0935) and an NSF CAREER Award (AGS 2047150) to SEP. IMD was supported by the Virginia Space Grant Consortium, University of Virginia College Science Scholars Program, and Double Hoo Research Award. MAGD was funded by a NASA Future Investigator NASA Earth and Space Science and Technology (FINESST) Graduate Research Fellowship (80NSSC20K1655) and the Virginia Space Grant Consortium. IMD, MAGD, KPF, and SEP acknowledge support from the University of Virginia Democracy Institute and the University of Virginia Repair Lab community of scholars. KS acknowledges support for the oversampling code development from the NASA Atmospheric Composition: Modeling and Analysis Program (80NSSC19K0988). Research Computing at UVA provided computational resources and technical support contributing to the results reported herein (https://rc.virginia.edu). All LISTOS datasets are freely accessible at: https://www-air.larc.nasa.gov/cgi-bin/ArcView/listos. We acknowledge the use of the publicly available TROPOMI NO_2 Level 2 vertical column densities (https://data-portal.s5p-pal.com/products/no2.html), U.S. Census database from the IPUMS National Historical Geographic Information System (https://www.nhgis.org), and TIGER/Line shapefiles of census tract polygons from the Data.gov library (https://www.census.gov/cgi-bin/geo/shapefiles/index.php). Hourly NO_2* and MDA8 O_3 mixing ratios were downloaded from the U.S. EPA file archive (https://www.epa.gov/outdoor-air-quality-data) and temperature surface winds speed observations were downloaded from the Iowa State University Iowa Environmental Mesonet download service (https://mesonet.agron.iastate.edu/request/download.phtml). The FIVE is publicly available at https://csl.noaa.gov/groups/csl7/measurements/2020covid-aqs/emissions/ and the NEI17 can be

downloaded at https://www.epa.gov/air-emissions-inventories/2017-national-emissions-inventory-nei-data.

Supporting Information Available. Study area maps, including example large and small LISTOS rasters, UA population density, and surface monitoring station locations. Figures displaying the distribution of TROPOMI pixel areas and variability in population demographics with different TROPOMI coverage levels. Tables describing LISTOS flight patterns, detailed LISTOS inequality results, correlations between LISTOS inequalities and various surface conditions, effect of pixel area on daily TROPOMI inequalities, influence of various factors on TROPOMI column-surface correlations, and relative weekday-weekend MDA8 O_3 NAAQS exceedances. The equation for population weighting and relationships between daily TROPOMI inequalities and various factors over O_3 season (May–September).

References

1. Maantay, J., Zoning law, health, and environmental justice: What's the connection? *Journal of Law Medicine & Ethics* **2002,** *30* (4), 572-+.

2. Maroko, A. R., Using air dispersion modeling and proximity analysis to assess chronic exposure to fine particulate matter and environmental justice in New York City. *Appl. Geogr.* **2012,** *34*, 533-547.

3. Maantay, J.; Maroko, A., Mapping Urban Risk: Flood Hazards, Race, & Environmental Justice In New York. *Appl. Geogr.* **2009,** *29* (1), 111-124.

4. Kheirbek, I.; Wheeler, K.; Walters, S.; Kass, D.; Matte, T., PM2.5 and ozone health impacts and disparities in New York City: sensitivity to spatial and temporal resolution. *Air Qual. Atmos. Health* **2013,** *6* (2), 473-486.

5. Kheirbek, I.; Haney, J.; Douglas, S.; Ito, K.; Matte, T., The contribution of motor vehicle emissions to ambient fine particulate matter public health impacts in New York City: a health burden assessment. *Environ. Health* **2016,** *15* (1).

6. McKane, R. G.; Satcher, L. A.; Houston, S. L.; Hess, D. J., Race, class, and space: an intersectional approach to environmental justice in New York City. *Environ. Sociol.* **2018,** *4* (1), 79-92.

7. Gilmore, J.; Mulgaonkar, P.; Oyewole, T. M.; Heimbinder, M. *Community Air Mapping for Environmental Justice*; New York City Environmental Justice Alliance: New York City Environmental Justice Alliance, 2021.

8. Sze, J., *Noxious New York : The Racial Politics of Urban Health and Environmental Justice*. MIT Press, 2007.

9. Ironbound Community Corporation. Picturing Justice. https://picturingjustice.tumblr.com (accessed January 7, 2022).

10. WEACT. WEACT History. http://old.weact.org/history.html (accessed August 14).

11. Clark, L. P.; Millet, D. B.; Marshall, J. D., National Patterns in Environmental Injustice and Inequality: Outdoor NO_2 Air Pollution in the United States. *PLOS ONE* **2014,** *9* (4), e94431.

12. Clark, L. P.; Millet, D. B.; Marshall, J. D., Changes in Transportation-Related Air Pollution Exposures by Race-Ethnicity and Socioeconomic Status: Outdoor Nitrogen Dioxide in the United States in 2000 and 2010. *Environ. Health Perspect.* **2017,** *125* (9).

13. Demetillo, M. A. G.; Harkins, C.; McDonald, B. C.; Chodrow, P. S.; Sun, K.; Pusede, S. E., Space-Based Observational Constraints on NO_2 Air Pollution Inequality From Diesel Traffic in Major US Cities. *Geophys. Res. Lett.* **2021,** *48* (17), e2021GL094333.

14. Kerr, G. H.; Goldberg, D. L.; Anenberg, S. C., COVID-19 pandemic reveals persistent disparities in nitrogen dioxide pollution. *Proc. Natl. Acad. Sci. U.S.A.* **2021,** *118* (30), e2022409118.

15. Tessum, C. W.; Apte, J. S.; Goodkind, A. L.; Muller, N. Z.; Mullins, K. A.; Paolella, D. A.; Polasky, S.; Springer, N. P.; Thakrar, S. K.; Marshall, J. D.; Hill, J. D., Inequity in consumption of goods and services adds to racial–ethnic disparities in air pollution exposure. *Proc. Natl. Acad. Sci. U.S.A.* **2019,** *116* (13), 6001-6006.

16. Chambliss, S. E.; Pinon, C. P. R.; Messier, K. P.; LaFranchi, B.; Upperman, C. R.; Lunden, M. M.; Robinson, A. L.; Marshall, J. D.; Apte, J. S., Local- and regional-scale racial and ethnic disparities in air pollution determined by long-term mobile monitoring. *Proc. Natl. Acad. Sci. U.S.A.* **2021,** *118* (37), e2109249118.

17. Demetillo, M. A. G.; Navarro, A.; Knowles, K. K.; Fields, K. P.; Geddes, J. A.; Nowlan, C. R.; Janz, S. J.; Judd, L. M.; Al-Saadi, J.; Sun, K.; McDonald, B. C.; Diskin, G. S.; Pusede, S. E., Observing Nitrogen Dioxide Air Pollution Inequality Using High-Spatial-Resolution Remote Sensing Measurements in Houston, Texas. *Environ. Sci. & Technol.* **2020,** *54* (16), 9882-9895

18. Apte, J. S.; Messier, K. P.; Gani, S.; Brauer, M.; Kirchstetter, T. W.; Lunden, M. M.; Marshall, J. D.; Portier, C. J.; Vermeulen, R. C. H.; Hamburg, S. P., High-Resolution Air Pollution Mapping with Google Street View Cars: Exploiting Big Data. *Environ. Sci. & Technol.* **2017,** *51* (12), 6999-7008.

19. Choi, W.; He, M. L.; Barbesant, V.; Kozawa, K. H.; Mara, S.; Winer, A. M.; Paulson, S. E., Prevalence of wide area impacts downwind of freeways under pre-sunrise stable atmospheric conditions. *Atmos. Environ.* **2012,** *62*, 318-327.

20. Karner, A. A.; Eisinger, D. S.; Niemeier, D. A., Near-Roadway Air Quality: Synthesizing the Findings from Real-World Data. *Environ. Sci. & Technol.* **2010,** *44* (14), 5334-5344.

21. Yu, K. A.; McDonald, B. C.; Harley, R. A., Evaluation of Nitrogen Oxide Emission Inventories and Trends for On-Road Gasoline and Diesel Vehicles. *Environ. Sci. & Technol.* **2021,** *55* (10), 6655-6664.

22. Harkins, C.; McDonald, B. C.; Henze, D. K.; Wiedinmyer, C., A fuel-based method for updating mobile source emissions during the COVID-19 pandemic. *Environ. Res. Lett.* **2021**, *16* 065018.

23. Travis, K. R.; Jacob, D. J.; Fisher, J. A.; Kim, P. S.; Marais, E. A.; Zhu, L.; Yu, K.; Miller, C. C.; Yantosca, R. M.; Sulprizio, M. P.; Thompson, A. M.; Wennberg, P. O.; Crounse, J. D.; St. Clair, J. M.; Cohen, R. C.; Laughner, J. L.; Dibb, J. E.; Hall, S. R.; Ullmann, K.; Wolfe, G. M.; Pollack, I. B.; Peischl, J.; Neuman, J. A.; Zhou, X., Why do models overestimate surface ozone in the Southeast United States? *Atmos. Chem. Phys.* **2016,** *16* (21), 13561-13577.

24. Southerland, V. A.; Anenberg, S. C.; Harris, M.; Apte, J.; Hystad, P.; Donkelaar, A. v.; Martin, R. V.; Beyers, M.; Roy, A., Assessing the Distribution of Air Pollution Health Risks

within Cities: A Neighborhood-Scale Analysis Leveraging High-Resolution Data Sets in the Bay Area, California. *Environ. Health Perspec.* **2021,** *129* (3), 037006.

25. Brook, J. R.; Burnett, R. T.; Dann, T. F.; Cakmak, S.; Goldberg, M. S.; Fan, X. H.; Wheeler, A. J., Further interpretation of the acute effect of nitrogen dioxide observed in Canadian time-series studies. *J. Expo. Sci. Environ. Epidemiol.* **2007,** *17*, S36-S44.

26. Brunekreef, B.; Holgate, S. T., Air pollution and health. *Lancet* **2002,** *360* (9341), 1233-1242.

27. Burnett, R. T.; Stieb, D.; Brook, J. R.; Cakmak, S.; Dales, R.; Raizenne, M.; Vincent, R.; Dann, T., Associations between short-term changes in nitrogen dioxide and mortality in Canadian cities. *Arch. Environ. Health* **2004,** *59* (5), 228-236.

28. Atkinson, R. W.; Butland, B. K.; Anderson, H. R.; Maynard, R. L., Long-term Concentrations of Nitrogen Dioxide and Mortality: A Meta-analysis of Cohort Studies. *Epidemio.* **2018,** *29* (4), 460-472.

29. Anenberg, S. C.; Henze, D. K.; Tinney, V.; Kinney, P. L.; Raich, W.; Fann, N.; Malley, C. S.; Roman, H.; Lamsal, L.; Duncan, B.; Martin, R. V.; Donkelaar, A. v.; Brauer, M.; Doherty, R.; Jonson, J. E.; Davila, Y.; Sudo, K.; Kuylenstierna, J. C. I., Estimates of the Global Burden of Ambient $PM_{2.5}$, Ozone, and NO_2 on Asthma Incidence and Emergency Room Visits. *Environ. Health Perspect.* **2018,** *126* (10), 107004.

30. Edwards, J.; Walters, S.; Griffiths, R. K., Hospital Admissions for Asthma in Preschool-Children–Relationship to Major Roads tn Birmingham, United-Kingdom. *Arch. Environ. Health* **1994,** *49* (4), 223-227.

31. Gauderman, W. J.; Avol, E.; Lurmann, F.; Kuenzli, N.; Gilliland, F.; Peters, J.; McConnell, R., Childhood asthma and exposure to traffic and nitrogen dioxide. *Epidemiol.* **2005,** *16* (6), 737-743.

32. Adar, S. D.; Kaufman, J. D., Cardiovascular disease and air pollutants: Evaluating and improving epidemiological data implicating traffic exposure. *Inhalation Toxicol.* **2007,** *19*, 135-149.

33. Lipfert, F. W.; Wyzga, R. E., On exposure and response relationships for health effects associated with exposure to vehicular traffic. *J. Expo. Sci. Environ. Epidemiol.* **2008,** *18* (6), 588-599.

34. Wu, J.; Ren, C. Z.; Delfino, R. J.; Chung, J.; Wilhelm, M.; Ritz, B., Association between Local Traffic-Generated Air Pollution and Preeclampsia and Preterm Delivery in the South Coast Air Basin of California. *Environ. Health Perspect.* **2009,** *117* (11), 1773-1779.

35. Lin, S.; Munsie, J. P.; Hwang, S.-A.; Fitzgerald, E.; Cayo, M. R., Childhood Asthma Hospitalization and Residential Exposure to State Route Traffic. *Environ. Res.* **2002,** *88* (2), 73-81.

36. Liu, J.; Clark, L. P.; Bechle, M. J.; Hajat, A.; Kim, S.-Y.; Robinson, A. L.; Sheppard, L.; Szpiro, A. A.; Marshall, J. D., Disparities in Air Pollution Exposure in the United States by Race/Ethnicity and Income, 1990-2010. *Environ. Health Perspect.* **2021,** *129* (12), 127005.

37. Goldberg, D. L.; Lu, Z.; Streets, D. G.; de Foy, B.; Griffin, D.; McLinden, C. A.; Lamsal, L. N.; Krotkov, N. A.; Eskes, H., Enhanced Capabilities of TROPOMI NO_2: Estimating NO_X from North American Cities and Power Plants. *Environ. Sci. & Technol.* **2019,** 53 (21), 12594-12601.

38. Griffin, D.; Zhao, X.; McLinden, C. A.; Boersma, F.; Bourassa, A.; Dammers, E.; Degenstein, D.; Eskes, H.; Fehr, L.; Fioletov, V.; Hayden, K.; Kharol, S. K.; Li, S.-M.; Makar, P.; Martin, R. V.; Mihele, C.; Mittermeier, R. L.; Krotkov, N.; Sneep, M.; Lamsal, L. N.; Linden, M. t.; Geffen, J. v.; Veefkind, P.; Wolde, M., High-Resolution Mapping of Nitrogen Dioxide With TROPOMI: First Results and Validation Over the Canadian Oil Sands. *Geophys. Res. Lett.* **2019,** *46* (2), 1049-1060.

39. Kowalewski, M. G.; Janz, S. J. In *Remote sensing capabilities of the GEO-CAPE airborne simulator*, SPIE Optical Engineering + Applications, SPIE: 2014; p 12.

40. Leitch, J. W.; Delker, T.; Good, W.; Ruppert, L.; Murcray, F.; Chance, K.; Liu, X.; Nowlan, C.; Janz, S. J.; Krotkov, N. A.; Pickering, K. E.; Kowalewski, M.; Wang, J. In *The GeoTASO airborne spectrometer project*, SPIE Optical Engineering + Applications, SPIE: 2014; p 9.

41. Nowlan, C. R.; Liu, X.; Leitch, J. W.; Chance, K.; González Abad, G.; Liu, C.; Zoogman, P.; Cole, J.; Delker, T.; Good, W.; Murcray, F.; Ruppert, L.; Soo, D.; Follette-Cook, M. B.; Janz, S. J.; Kowalewski, M. G.; Loughner, C. P.; Pickering, K. E.; Herman, J. R.; Beaver, M. R.; Long, R. W.; Szykman, J. J.; Judd, L. M.; Kelley, P.; Luke, W. T.; Ren, X.; Al-Saadi, J. A., Nitrogen dioxide observations from the Geostationary Trace gas and Aerosol Sensor Optimization (GeoTASO) airborne instrument: Retrieval algorithm and measurements during DISCOVER-AQ Texas 2013. *Atmos. Meas. Tech.* **2016,** *9* (6), 2647-2668.

42. Nowlan, C. R.; Liu, X.; Janz, S. J.; Kowalewski, M. G.; Chance, K.; Follette-Cook, M. B.; Fried, A.; González Abad, G.; Herman, J. R.; Judd, L. M.; Kwon, H. A.; Loughner, C. P.; Pickering, K. E.; Richter, D.; Spinei, E.; Walega, J.; Weibring, P.; Weinheimer, A. J., Nitrogen dioxide and formaldehyde measurements from the GEOstationary Coastal and Air Pollution Events (GEO-CAPE) Airborne Simulator over Houston, Texas. *Atmos. Meas. Tech.* **2018,** *11* (11), 5941-5964.

43. Judd, L. M.; Al-Saadi, J. A.; Janz, S. J.; Kowalewski, M. G.; Pierce, R. B.; Szykman, J. J.; Valin, L. C.; Swap, R.; Cede, A.; Mueller, M.; Tiefengraber, M.; Abuhassan, N.; Williams, D., Evaluating the impact of spatial resolution on tropospheric NO_2 column comparisons within urban areas using high-resolution airborne data. *Atmos. Meas. Tech.* **2019,** *12* (11), 6091-6111.

44. Judd, L. M.; Al-Saadi, J. A.; Szykman, J. J.; Valin, L. C.; Janz, S. J.; Kowalewski, M. G.; Eskes, H. J.; Veefkind, J. P.; Cede, A.; Mueller, M.; Gebetsberger, M.; Swap, R.; Pierce, R. B.; Nowlan, C. R.; Abad, G. G.; Nehrir, A.; Williams, D., Evaluating Sentinel-5P TROPOMI

tropospheric NO_2 column densities with airborne and Pandora spectrometers near New York City and Long Island Sound. *Atmos. Meas. Tech.* **2020,** *13,* 6113–6140.

45. Prather, M., Catastrophic loss of stratospheric ozone in dense volcanic clouds. *Geophys. Res.-Atmos* **1992,** *97*, 10187–10191.

46. McLinden, C. A.; Olsen, S. C.; Hannegan, B.; Wild, O.; Prather, M. J.; Sundet, J., Stratospheric ozone in 3-D models: A simple chemistry and the cross-tropopause flux. *J. Geophys. Res.: Atmos.* **2000,** *105* (D11), 14653-14665.

47. Stajner, I. D., Paula; Byun, Daewon; McQueen, Jeffery; Draxler, Roland; Dickerson, Phil; Meagher, James, US National Air Quality Forecast Capability: Expanding Coverage to Include Particulate Matter. In *Air Pollution Modeling and its Application,* XXI; Elsevier Science, 2011.

48. van Geffen, J. H. G.; Boersma, K. F.; Eskes, H. J.; Maasakkers, J. D.; Veefkind, J. P. TROPOMI ATBD of the total and tropospheric NO_2 data products. http://www.tropomi.eu (accessed 12 May).

49. Veefkind, J. P.; Aben, I.; McMullan, K.; Förster, H.; de Vries, J.; Otter, G.; Claas, J.; Eskes, H. J.; de Haan, J. F.; Kleipool, Q.; van Weele, M.; Hasekamp, O.; Hoogeveen, R.; Landgraf, J.; Snel, R.; Tol, P.; Ingmann, P.; Voors, R.; Kruizinga, B.; Vink, R.; Visser, H.; Levelt, P. F., TROPOMI on the ESA Sentinel-5 Precursor: A GMES mission for global observations of the atmospheric composition for climate, air quality and ozone layer applications. *Remote Sens. Environ.* **2012,** *120*, 70-83.

50. Boersma, K. F.; Eskes, H. J.; Dirksen, R. J.; van der A, R. J.; Veefkind, J. P.; Stammes, P.; Huijnen, V.; Kleipool, Q. L.; Sneep, M.; Claas, J.; Leitão, J.; Richter, A.; Zhou, Y.; Brunner, D., An improved tropospheric NO_2 column retrieval algorithm for the Ozone Monitoring Instrument. *Atmos. Meas. Tech.* **2011,** *4* (9), 1905-1928.

51. Boersma, K. F.; Eskes, H. J.; Richter, A.; De Smedt, I.; Lorente, A.; Beirle, S.; van Geffen, J. H. G. M.; Zara, M.; Peters, E.; Van Roozendael, M.; Wagner, T.; Maasakkers, J. D.; van der A, R. J.; Nightingale, J.; De Rudder, A.; Irie, H.; Pinardi, G.; Lambert, J. C.; Compernolle, S. C., Improving algorithms and uncertainty estimates for satellite NO_2 retrievals: results from the quality assurance for the essential climate variables (QA4ECV) project. *Atmos. Meas. Tech.* **2018,** *11* (12), 6651-6678.

52. Lorente, A.; Folkert Boersma, K.; Yu, H.; Dörner, S.; Hilboll, A.; Richter, A.; Liu, M.; Lamsal, L. N.; Barkley, M.; De Smedt, I.; Van Roozendael, M.; Wang, Y.; Wagner, T.; Beirle, S.; Lin, J. T.; Krotkov, N.; Stammes, P.; Wang, P.; Eskes, H. J.; Krol, M., Structural uncertainty in air mass factor calculation for NO_2 and HCHO satellite retrievals. *Atmos. Meas. Tech.* **2017,** *10* (3), 759-782.

53. van Geffen, J. H. G. M.; Boersma, K. F.; Van Roozendael, M.; Hendrick, F.; Mahieu, E.; De Smedt, I.; Sneep, M.; Veefkind, J. P., Improved spectral fitting of nitrogen dioxide from OMI in the 405–465 nm window. *Atmos. Meas. Tech.* **2015,** *8* (4), 1685-1699.

54. Zara, M.; Boersma, K. F.; De Smedt, I.; Richter, A.; Peters, E.; van Geffen, J. H. G. M.; Beirle, S.; Wagner, T.; Van Roozendael, M.; Marchenko, S.; Lamsal, L. N.; Eskes, H. J., Improved slant column density retrieval of nitrogen dioxide and formaldehyde for OMI and GOME-2A from QA4ECV: intercomparison, uncertainty characterisation, and trends. *Atmos. Meas. Tech.* **2018,** *11* (7), 4033-4058.

55. Boersma, K. F.; Eskes, H. J.; Brinksma, E. J., Error analysis for tropospheric NO_2 retrieval from space. *J. Geophys. Res.: Atmos.* **2004,** *109* (D4).

56. Kleipool, Q. L.; Dobber, M. R.; de Haan, J. F.; Levelt, P. F., Earth surface reflectance climatology from 3 years of OMI data. *J. Geophys. Res.-Atmos.* **2008,** *113* (D18).

57. Williams, J. E.; Boersma, K. F.; Le Sager, P.; Verstraeten, W. W., The high-resolution version of TM5-MP for optimized satellite retrievals: description and validation. *Geosci. Model Dev.* **2017,** *10* (2), 721-750.

58. Ludewig, A.; Kleipool, Q.; Bartstra, R.; Landzaat, R.; Leloux, J.; Loots, E.; Meijering, P.; van der Plas, E.; Rozemeijer, N.; Vonk, F.; Veefkind, P., In-flight calibration results of the TROPOMI payload on board the Sentinel-5 Precursor satellite. *Atmos. Meas. Tech.* **2020,** *13* (7), 3561-3580.

59. Sun, K.; Zhu, L.; Cady-Pereira, K.; Chan Miller, C.; Chance, K.; Clarisse, L.; Coheur, P. F.; González Abad, G.; Huang, G.; Liu, X.; Van Damme, M.; Yang, K.; Zondlo, M., A physics-based approach to oversample multi-satellite, multispecies observations to a common grid. *Atmos. Meas. Tech.* **2018,** *11* (12), 6679-6701.

60. Spielman, S. E.; Folch, D.; Nagle, N., Patterns and causes of uncertainty in the American Community Survey. *Appl. Geogr.* **2014,** *46*, 147-157.

61. U.S. Census Bureau, *Understanding and Using American Community Survey Data: What All Data Users Need to Know*; Washington, DC, 2020.

62. Winer, A. M.; Peters, J. W.; Smith, J. P.; Pitts, J. N., Response of commercial chemiluminescent nitric oxide-nitrogen dioxide analyzers to other nitrogen-containing compounds. *Environ. Sci. & Technol.* **1974,** *8* (13), 1118-1121.

63. Dunlea, E. J.; Herndon, S. C.; Nelson, D. D.; Volkamer, R. M.; San Martini, F.; Sheehy, P. M.; Zahniser, M. S.; Shorter, J. H.; Wormhoudt, J. C.; Lamb, B. K.; Allwine, E. J.; Gaffney, J. S.; Marley, N. A.; Grutter, M.; Marquez, C.; Blanco, S.; Cardenas, B.; Retama, A.; Ramos Villegas, C. R.; Kolb, C. E.; Molina, L. T.; Molina, M. J., Evaluation of nitrogen dioxide chemiluminescence monitors in a polluted urban environment. *Atmos. Chem. Phys.* **2007,** *7* (10), 2691-2704.

64. Steinbacher, M.; Zellweger, C.; Schwarzenbach, B.; Bugmann, S.; Buchmann, B.; Ordóñez, C.; Prevot, A. S. H.; Hueglin, C., Nitrogen oxide measurements at rural sites in Switzerland: Bias of conventional measurement techniques. *J. Geophys. Res.-Atmos.* **2007,** *112* (D11).

65. McDonald, B. C.; Dallmann, T. R.; Martin, E. W.; Harley, R. A., Long-term trends in nitrogen oxide emissions from motor vehicles at national, state, and air basin scales. *J. Geophys. Res.-Atmos.* **2012,** *117* (D21).

66. McDonald, B. C.; McKeen, S. A.; Cui, Y. Y.; Ahmadov, R.; Kim, S.-W.; Frost, G. J.; Pollack, I. B.; Peischl, J.; Ryerson, T. B.; Holloway, J. S.; Graus, M.; Warneke, C.; Gilman, J. B.; de Gouw, J. A.; Kaiser, J.; Keutsch, F. N.; Hanisco, T. F.; Wolfe, G. M.; Trainer, M., Modeling Ozone in the Eastern U.S. using a Fuel-Based Mobile Source Emissions Inventory. *Environ. Sci. & Technol.* **2018,** *52* (13), 7360-7370.

67. Frost, G. J.; McKeen, S. A.; Trainer, M.; Ryerson, T. B.; Neuman, J. A.; Roberts, J. M.; Swanson, A.; Holloway, J. S.; Sueper, D. T.; Fortin, T.; Parrish, D. D.; Fehsenfeld, F. C.; Flocke, F.; Peckham, S. E.; Grell, G. A.; Kowal, D.; Cartwright, J.; Auerbach, N.; Habermann, T., Effects of changing power plant NO_x emissions on ozone in the eastern United States: Proof of concept. *J. Geophys. Res.-Atmos.* **2006,** *111* (D12).

68. Jiang, Z.; McDonald, B. C.; Worden, H.; Worden, J. R.; Miyazaki, K.; Qu, Z.; Henze, D. K.; Jones, D. B. A.; Arellano, A. F.; Fischer, E. V.; Zhu, L.; Boersma, K. F., Unexpected slowdown of US pollutant emission reduction in the past decade. *Proc. Natl. Acad. Sci. U.S.A.* **2018,** *115* (20), 5099-5104.

69. York, D.; Evensen, N. M.; Martínez, M. L.; Delgado, J. D. B., Unified equations for the slope, intercept, and standard errors of the best straight line. *Amer. J. Phys.* **2004,** *72* (3), 367-375.

70. Chodrow, P. S., Structure and information in spatial segregation. *Proc. Natl. Acad. Sci. U.S.A.* **2017,** *114* (44), 11591-11596.

71. Eskes, H. J., van Geffen, J., Sneep, M., Veefkind, J. P., Niemeier, S., Zehner, C., S5P Nitrogen Dioxide v02.03.01 intermediate reprocessing on the S5P-PAL system: Readme file. 2021.

72. Bechle, M. J.; Millet, D. B.; Marshall, J. D., Remote sensing of exposure to NO_2: Satellite versus ground-based measurement in a large urban area. *Atmos. Environ.* **2013,** *69*, 345-353.

73. Jin, X.; Fiore, A.; Boersma, K. F.; Smedt, I. D.; Valin, L., Inferring Changes in Summertime Surface Ozone–NO_x–VOC Chemistry over U.S. Urban Areas from Two Decades of Satellite and Ground-Based Observations. *Environ. Sci. & Technol.* **2020,** *54* (11), 6518-6529.

74. Liu, J.; Clark, L. P.; Bechle, M. J.; Hajat, A.; Kim, S. Y.; Robinson, A. L.; Sheppard, L.; Szpiro, A. A.; Marshall, J. D., Disparities in Air Pollution Exposure in the United States by Race/Ethnicity and Income, 1990-2010. *Environ. Health Perspect.* **2021,** *129* (12), 127005.

75. Pusede, S. E.; Cohen, R. C., On the observed response of ozone to NO_x and VOC reactivity reductions in San Joaquin Valley California 1995-present. *Atmos. Chem. Phys.* **2012,** *12* (18), 8323-8339.

76. Leibensperger, E. M.; Mickley, L. J.; Jacob, D. J., Sensitivity of US air quality to mid-latitude cyclone frequency and implications of 1980–2006 climate change. *Atmos. Chem. Phys.* **2008,** *8* (23), 7075-7086.

77. Mickley, L. J.; Jacob, D. J.; Field, B. D.; Rind, D., Climate response to the increase in tropospheric ozone since preindustrial times: A comparison between ozone and equivalent CO2 forcings. *J. Geophys. Res.-Atmos.* **2004,** *109* (D5).

78. Reidmiller, D. R.; Avery, C. W.; Easterling, D. R.; Kunkel, K. E.; Lewis, K. L. M.; Maycock, T. K.; Stewart, B. C., Impacts, Risks, and Adaptation in the United States: Fourth National Climate Assessment, Volume II., 2017.

79. Harvey, B. J.; Cook, P.; Shaffrey, L. C.; Schiemann, R., The Response of the Northern Hemisphere Storm Tracks and Jet Streams to Climate Change in the CMIP3, CMIP5, and CMIP6 Climate Models. *J. Geophys. Res.-Atmos.* **2020,** *125* (23), e2020JD032701.

80. Horton, D. E.; Skinner, C. B.; Singh, D.; Diffenbaugh, N. S., Occurrence and persistence of future atmospheric stagnation events. *Nat. Clim. Chang.* **2014,** *4* (8), 698-703.

81. Turner, A. J.; Fiore, A. M.; Horowitz, L. W.; Bauer, M., Summertime cyclones over the Great Lakes Storm Track from 1860–2100: variability, trends, and association with ozone pollution. *Atmos. Chem. Phys.* **2013,** *13* (2), 565-578.

82. Klein Rosenthal, J.; Kinney, P. L.; Metzger, K. B., Intra-urban vulnerability to heat-related mortality in New York City, 1997–2006. *Health & Place* **2014,** *30*, 45-60.

83. Chakraborty, T.; Hsu, A.; Manya, D.; Sheriff, G., Disproportionately higher exposure to urban heat in lower-income neighborhoods: a multi-city perspective. *Environ. Res. Lett.* **2019,** *14* (10), 105003.

84. Mitchell, B. C.; Chakraborty, J., Landscapes of thermal inequity: disproportionate exposure to urban heat in the three largest US cities. *Environ. Res. Lett.* **2015,** *10* (11), 115005.

85. Gilmore, J.; Mulgaonkar, P.; Oyewole, T. M.; Heimbinder, M. CAMP-EJ: Community Mapping Project for Environmental Justice: Findings & Recommendations Report; February 2021.

86. Stewart-Cousins, A.; Addabbo Jr, J. P.; Biaggi, A.; Bailey, J. T.; Brouk, S. G., An act to amend the environmental conservation law, in relation to the location of environmental facilities. 2021.

87. New Jersey's Environmental Justice Law. In *13*, State and General Assembly of the State of New Jersey: 2020.

For Table of Contents Only: